Does direct impact of SST on short wind waves matter for scatterometry?

Semyon A. Grodsky,[1] Vladimir N. Kudryavtsev,[2] Abderrahim Bentamy,[3] James A. Carton,[1] and Bertrand Chapron[2,3]

Received 19 April 2012; revised 18 May 2012; accepted 21 May 2012; published 20 June 2012.

[1] Scatterometer radar backscatter depends on the relationship linking surface stress and surface roughness. SST can alter the growth rate of centimeter-scale waves through its impact on air and water density and water viscosity. This SST-dependency has *not* been included in the standard Geophysical Model Functions. This study uses a radar imaging model to evaluate this SST-dependence and compares the results to observations from QuikScat Ku-band and ASCAT C-band scatterometers. A SST correction could raise wind speeds by up to 0.2 ms^{-1} in the storm track region of the Southern Ocean for C-band scatterometers. For the higher frequency Ku-band scatterometers, a SST-induced reduction up to 0.4 ms^{-1} is predicted south of 60°S, where SST is cold and winds are moderate. **Citation:** Grodsky, S. A., V. N. Kudryavtsev, A. Bentamy, J. A. Carton, and B. Chapron (2012), Does direct impact of SST on short wind waves matter for scatterometry?, *Geophys. Res. Lett.*, *39*, L12602, doi:10.1029/2012GL052091.

1. Introduction

[2] Scatterometry has revolutionized analysis of marine winds, but climate quality intercalibration of scatterometer winds remains a research problem. *Bentamy et al.* [2012] compared wind estimates from two scatterometers operating at Ku- and C-band frequencies and found a systematic pattern of mean difference whose geographic distribution seemingly is related to the mean distribution of SST. Beyond the known impact of SST variations on mesoscale wind variations, in particular via the stability of the marine atmospheric boundary layer (see *Chelton and Xi*e [2010] for a review), Bentamy and co-authors speculated that these scatterometer differences resulted from neglecting the direct impact of SST on atmospheric momentum and oceanic viscous dissipation processes affecting ocean surface wave generation/dissipation.

[3] Indeed, separate from the impact of SST gradients via the atmospheric boundary layer wind transformations [e.g., *Weissman et al.*, 1980; *Beal et al.*, 1997], SST can also directly impact the growth rate and geometry of wind waves, and thus sea surface radar backscatter. Scatterometers measure wind velocity indirectly through the spectrum of centimeter-scale wind waves. The spectrum of these waves depends on the wind growth rate, β_w, which in turn is proportional to the ratio of air to water density, ρ_a/ρ_w [e.g., *Donelan and Pierson*, 1987]. Hence, rougher seas are generated by denser air over cold SSTs, assuming that the wind friction velocity itself remains unchanged [*Bourassa et al.*, 2010]. But, smoother waves are also expected due to higher viscosity, ν, and stronger viscous dissipation, β_ν, for colder water. Thus, for fixed winds, wave energy and radar backscatter may either increase or decrease with SST due to changes in β_w and β_ν.

[4] To date, the most successful conversions of scatterometer measurements to near-surface wind rely on empirically derived geophysical model functions (GMFs). In particular, the National Aeronautics and Space Administration (NASA) QuikSCAT uses frequencies in the 10.95–14.5 GHz Ku-band while European scatterometers have all adopted the 4–8 GHz C-band to reduce sensitivity to rain interference [e.g., *Sobieski et al*, 1999]. The NASA Ku-band winds are estimated with the empirical QSCAT-1 GMF [*Dunbar et al.*, 2006]. The European Meteorological Satellite Organization (EUMETSAT) C-band winds are estimated with the empirical CMOD5N GMF [*Hersbach*, 2008]. Although neither GMFs account for SST variations, careful tuning of the GMFs provides an accuracy of 10 m neutral wind velocity in the range of ± 1 ms^{-1} and $\pm 20°$ [e.g. *Ebuchi et al.*, 2002]. Yet, within these ranges of error, systematic errors emerge at high latitudes over very cold SST < 5°C [*Bentamy et al.*, 2012]. In this paper, we employ the *Kudryavtsev et al.* [2005] Radar Imaging Model (RIM) to evaluate sensitivity differences in scatterometer winds arising from the lack of SST-dependence in current GMFs.

2. Collocated Scatterometer Data

[5] This study relies on a set of observed differences between spatially and temporally collocated 10 m neutral winds $\Delta W = W_{QS} - W_{AS}$ from the Ku-band (13.4 GHz, 2.24 cm) SeaWinds instrument onboard QuikSCAT (referred to as QuikSCAT or QS) and the C-band (5.225 GHz, 5.74 cm) ASCAT (referred to as ASCAT or AS) onboard EUMETSAT MetOp-A. The collocated winds are separated by less than 4 hours and 50 km, during the November 2008 – November 2009 period when ASCAT processing used the current CMOD5N GMF to derive 10 m neutral wind.

3. Radar Imaging Model

[6] The *Kudryavtsev et al.* [2005] RIM simulates the normalized radar cross section, $\sigma_0 = \sigma^0_{BR} + \sigma^0_{SP} + \sigma^0_{WB}$, by

[1]Department of Atmospheric and Oceanic Science, University of Maryland, College Park, Maryland, USA.
[2]Nansen International Environmental and Remote Sensing Centre, Russian State Hydrometeorological University, St. Petersburg, Russia.
[3]Institut Francais pour la Recherche et l'Exploitation de la Mer, Plouzane, France.

Corresponding author: S. A. Grodsky, Department of Atmospheric and Oceanic Science, University of Maryland, College Park, MD 20742, USA. (senya@atmos.umd.edu)

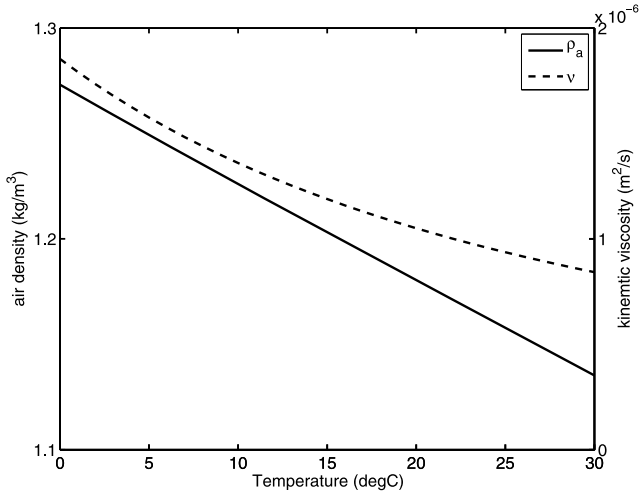

Figure 1. Air density (ρ_a) and sea water kinematic viscosity (ν) versus temperature. Air density is calculated at the normal air pressure and relative humidity of 75%. Kinematic viscosity is calculated at constant salinity of 35 psu.

accounting for two-scale Bragg scattering, σ^0_{BR}, specular reflections, σ^0_{SP}, and scattering by wave breaking, σ^0_{WB}. This model is a practical tool in line with more advanced scattering models to extend Physical Optics (PO) solutions [*Voronovich and Zavorotny*, 2001; *Mouche et al.*, 2007]. In contrast to Bragg scattering, PO contributions from the specular reflections and very rough radar detected surface patterns associated with macro- and micro-scale wave breaking are independent of polarization. Regular specular reflection, σ^0_{SP}, is weak in the range of incidence angles, θ, utilized by scatterometers, but σ^0_{WB} is not negligible. Transient rough wave breakings generate a strong local radar signal. Though their fraction is small, these zones nevertheless significantly contribute to σ^0, especially for H-pol radar signals. Centimeter-scale Bragg waves can also be generated from longer (a few decimeters or more) wave breaking events, that are less dependent on SST than the resonant Bragg waves.

[7] Following *Donelan and Pierson* [1987] and *Kudryavtsev et al.* [1999], the wave spectrum in the equilibrium range, $S(\vec{k})$, is balanced by the wind forcing, viscous dissipation (first term in 1), and nonlinear dissipation (second term in 1). In *Kudryavtsev et al.* [2005], the energy input due to breaking of longer waves, I_{wb}, is further added [*Kudryavtsev and Johannessen*, 2004], leading to the simplified balance equation:

$$\beta B(\vec{k}) - B(\vec{k})[B(\vec{k})/\alpha]^n + I_{wb}(\vec{k}) = 0, \tag{1}$$

where $B(\vec{k}) = k^4 S(\vec{k})$ is the saturation spectrum of wind waves, and α and n are empirical parameters. The growth rate, $\beta = \beta_w - \beta_\nu$, is the difference between the wind growth rate, β_w, and the rate of viscous dissipation, $\beta_\nu = 4\nu k^2/\omega$. The wind growth rate (2) is parameterized in a functional form suggested by *Stewart* [1974]

$$\beta_w = 1.5 \frac{\rho_a}{\rho_w} \frac{u_*(W_{\pi/k} - c)}{c^2} |\cos(\varphi)| \cos(\varphi), \tag{2}$$

where φ is the angle between wind and wave azimuth, k is the wavenumber, u_* is the air friction velocity, $W_{\pi/k}$ is wind speed at $z = \pi/k$, $c = \omega/k$, is the phase velocity, and $\omega = (gk + \gamma k^3)^{0.5}$ is the wave frequency that depends weakly on SST via its impact on surface tension γ. The drag coefficient is parameterized via the roughness length [*Smith*, 1988], $z_0 = 0.1\nu/u_* + 0.012u_*^2 / g$, which is valid for winds below 26 ms^{-1}.

[8] Centimeter scale wind waves are generated by air-sea interactions within a few centimeter thick layer just above the sea surface. The air temperature, T_a, within this layer is very close to SST. Its effect on the wind growth rate (2) is accounted for by the air density $\rho_a(T_a)$, which is calculated at normal air pressure and saturated humidity defined by SST. The water temperature, T_w, effect on β_ν is accounted for by the kinematic viscosity $\nu(T_w)$ that is calculated at fixed salinity of 35 psu [*Sharqawy et al.*, 2010]. Friction velocity u_* and wind speed $W_{\pi/k}$ in (2) are calculated using a neutral drag coefficient. With these parameterizations, the RIM produces $\sigma^0(W, T)$ that reasonably fits measurements in the observed range of winds, and for a given wind, W, now depends on temperature, T. Because current GMFs don't depend on SST, the radar calibration, $\sigma^0(W, T_0)$, refers to a temperature T_0 chosen equal the global mean SST = 19°C. The temperature-related wind retrieval error becomes

$$dW = \frac{\sigma^0(W,T) - \sigma^0(W,T_0)}{\left.\frac{\partial\sigma^0}{\partial W}\right|_{T_0}} \tag{3}$$

4. Results

[9] Although ρ_a decreases by approximately 10% between 0°C to 30°C (Figure 1) while ν drops by 50%, the impact of changes in these two factors on dW are comparable. In Figure 2 the two contributions to wind retrieval error (dW_ρ) and (dW_ν) are evaluated from (3) by varying either ρ_a or ν as a function of the surface temperature, keeping the other variable fixed at its value for T_0 = 19°C. The errors in Figure 2 are illustrated for the extreme case of cold SST, T_w = 0°C. The error in the wind estimates due to air density changes, dW_ρ, is mostly positive at these conditions because of denser air (in comparison with that at T_0). It increases quasi-linearly with W and is virtually independent of the radar wavelength. Neglecting the wave breaking impact, the σ^0 is dominated by the Bragg scattering and directly depends on $\beta = \beta_w - \beta_\nu$. A Taylor series expansion of (3) in vicinity of T_0 yields:

$$dW = dW_\rho + dW_\nu = \frac{\Delta\rho_a}{\rho_a} \left.\frac{\beta_w}{\partial\beta_w/\partial W}\right|_{T_0} - \frac{\Delta\nu}{\nu} \left.\frac{\beta_\nu}{\partial\beta_w/\partial W}\right|_{T_0} \tag{4}$$

[10] If $\beta_w \sim W^m$ the first term in (4) is linear in wind, $dW_\rho = (\Delta\rho_a/\rho_a)W$. For the wind growth rate model (2), dW_ρ is quasi-linear in wind with minor dependence on radar wavelength (Figure 2) that refers to the wavenumber dependence of $W_{\pi/k} - c$. Owing to the viscous dissipation, dW_ρ becomes negative for 10 m winds $W < 4$ ms^{-1} as the near-surface wind $W_{\pi/k}$ drops below the Bragg component phase speed, $W_{\pi/k} < c$, see (2). At those low winds, direct interaction with wind extracts energy from the surface waves at a rate proportional to ρ_a.

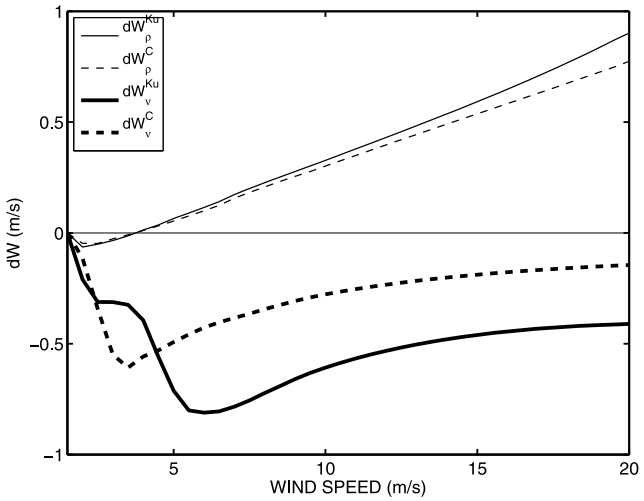

Figure 2. Wind retrieval error at SST = 0°C in Ku- and C-band due to SST-induced variations in the air density (dW_ρ) and water viscosity (dW_ν). Radar calibration ($\partial\sigma^0/\partial W$) is assumed corresponding to the global mean SST = 19°C. Data correspond to V-pol, upwind, $\theta = 45°$.

[11] In contrast to the impact of neglecting temperature-dependence in ρ_a, the impact of neglecting SST-dependence in ν is to cause a wind underestimation over cold water, $dW_\nu < 0$ (Figure 2). Although the two effects tend to cancel each other, they have different wind dependencies. In the C-band $|dW_\rho| < |dW_\nu|$ at low to moderate winds ($W < 13$ m/s) while $|dW_\rho| > |dW_\nu|$ at higher winds.

[12] The magnitude $|dW_\nu|$ is larger at shorter wavelengths where viscosity has more impact (Figure 2). But, this relationship switches over at $W < 5$ ms^{-1}. The RIM shows that in the Ku-band σ^0_{BR} dominates the V-pol component of σ^0 in the upwind direction at $W > 4$ ms^{-1}. But, as W decreases toward the threshold wind for the resonant Bragg component (defined by $\beta = 0$), which is approximately 4 ms^{-1} in the Ku band, Bragg scattering decreases sharply and drops below σ_{WB}. This results in a weaker temperature dependence of σ^0, now mostly dominated by an overall sea state roughness, less directly dependent on ν, thus on SST. The threshold wind to input energy at the C-band resonant wavelength is lower (~2.5 ms^{-1}) than that in the Ku-band, consistent with a much smaller β_ν for short gravity waves. As a result, $|dW_\nu^{Ku}| < |dW_\nu^{C}|$ under low winds <5 ms^{-1}.

[13] Observed collocated wind speed difference from QuikSCAT and ASCAT, $\Delta W = W_{AS} - W_{QS}$, is binned in Figure 3a as a function of the ECMWF operational analysis wind speed W and SST. Positive ΔW for $W > 15$ ms^{-1} has been attributed to the difference in QuikSCAT and ASCAT GMFs [*Bentamy et al.*, 2012], while positive ΔW for $W < 3$ ms^{-1} is an artifact of the asymmetrical distribution of wind speed for winds approaching the low wind cutoff [*Freilich*, 1997]. These positive ΔW can not be explained by the model, which accounts only for the physics of radar backscattering.

[14] For model comparison to observations we consider winds in the range 5 ms^{-1} < W < 12 ms^{-1}. Over cold SST < 7°C, W_{AS} exceeds W_{QS} by at least 0.25 ms^{-1}, due to a stronger viscous dissipation in the Ku- than the C-band (Figure 3a). The area of negative ΔW also shows up at finer collocations (time separation <1 hour, Figure 3b) but is based only on a small fraction (<7%) of the original collocations. The model predicts a qualitatively similar impact of SST at cold SST < 10°C and moderate winds (Figure 3c). The simulated $\Delta W < 0$ extends into higher winds

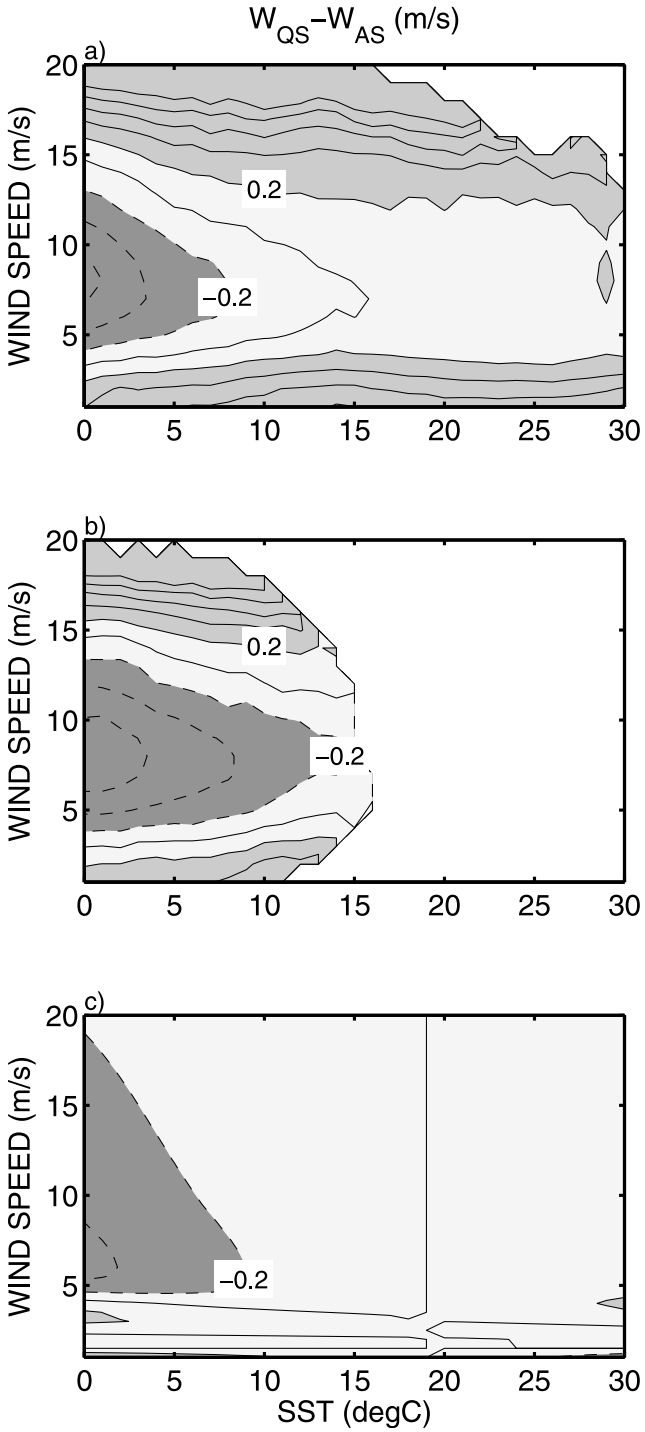

Figure 3. (a) Collocated QuikSCAT-ASCAT (November 2008-November 2009) wind speed difference ($W_{QS} - W_{AS}$) binned 1° in SST and 1 ms^{-1} in W. (b) The same as in Figure 3a but for temporal separations $\tau < 1$ hr (6.5% of collocations). Bins with less than 2,000 collocations are blanked. (c) Wind speed difference based on the *Kudryavtsev et al.* [2005] radar imaging model (vertical polarization, upwind direction, $\theta = 45°$). CI = 0.2 m/s.

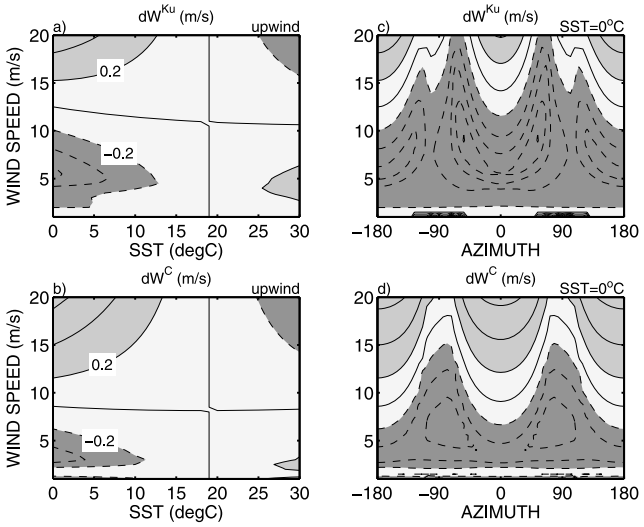

Figure 4. SST-related errors in wind speed retrievals (dW) evaluated using the radar imaging model and (3) at V-pol, and $\theta = 45°$ for (a, c) Ku-band and (b, d) C-band. Figures 4a and 4b show dW as a function of SST and W for radar antenna looking in the upwind direction. Figures 4c and 4d show dW as a function of radar antenna azimuth relative to wind direction and W and for SST = 0°C. Radar calibration is assumed to be corresponding to the global mean SST of $T_0 = 19$°C. In Figures 4c and 4d zero azimuth corresponds to radar antenna looking in the downwind direction. CI = 0.2 m/s.

$W > 15$ ms^{-1} for cold SSTs but can't be verified by observations dominated by the GMF-related effects at high winds. At the very cold SST = 0°C, the model predicts weaker $\Delta W = -0.4$ ms^{-1} in comparison with observed values of -0.6 ms^{-1} (Figure 3). In part, these differences are expected because the model results presented here are based on a particular set of parameters (V-pol., upwind direction, and $\theta = 45°$) while the scatterometer data result from observations at various angles and polarizations.

[15] In the upwind direction the wind retrieval error, dW, has a similar dependence on W and SST in either frequency band (Figures 4a and 4b). As defined, $dW(T = 19°C) = 0$, becoming approximately anti-symmetric with respect to T_0 at higher and lower temperatures with some modifications due to the stronger impact of $\nu(T_w)$ (Figure 1) at colder SSTs. For the Ku-band, viscous effects dominate at $W < 13$ ms^{-1} (Figure 4a). As expected, this negative dW is weaker for the C-band and limited to winds <9 ms^{-1} (Figure 4b). The positive dW at high winds is also stronger in the C-band due to weaker viscous effects at longer wavelengths (Figure 2).

[16] Azimuthal dependence of dW is approximately symmetrical in the downwind and upwind directions for conditions where Bragg scattering dominates. Any deviation from this symmetry is explained by σ_{WB}, which is less temperature dependent than Bragg scattering, and is stronger in the upwind direction. So, looking downwind in the Ku-band shows that dW is stronger than upwind (Figure 4c) due to a weaker σ_{WB} downwind. The upwind- downwind asymmetry of dW is less noticeable in the C-band (Figure 4d) due to the relatively stronger Bragg scattering in that band. In general the strongest negative dW is expected within the $\pm 90°$ downwind azimuth sector at some angles relative to the wind direction where the relative magnitude of azimuth-independent β_ν is stronger in comparison with azimuth-dependent β_w (Figures 4c and 4d).

[17] Differences in dW between the two radar bands are reflected in the geographical patterns of the wind retrieval error (Figure 5). These patterns are calculated from (3) assuming the upwind direction for V-pol and $\theta = 45°$, and using observed ASCAT neutral wind speed and ECMWF SST from the triplet collocated QuikSCAT/ASCAT/ECMWF data. The results are binned in a $1° \times 1°$ longitude/latitude grid and time average at each point. The density error

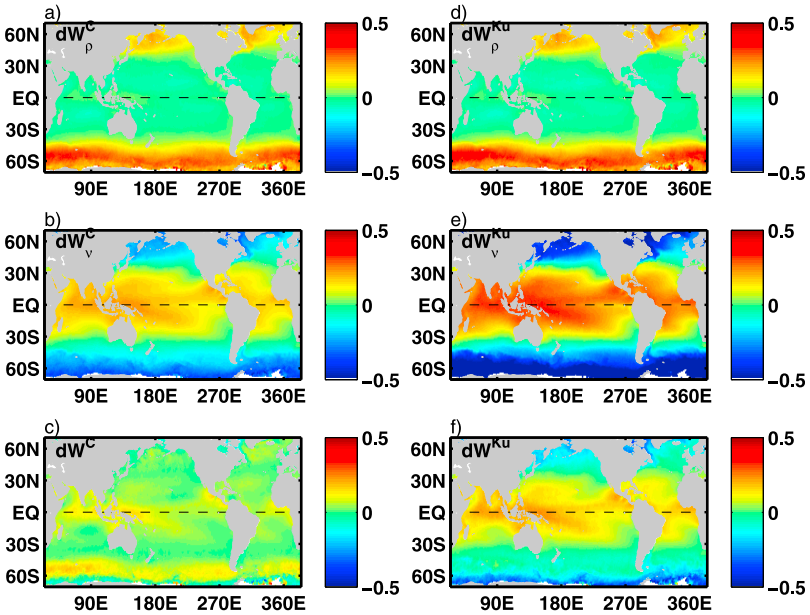

Figure 5. Spatial distribution of model wind retrieval errors in (left) C-band, (right) Ku-band. (a, d) Error due to SST-induced variation in air density (ρ_a), (b, e) error due to SST-induced variation in water viscosity (ν), (c, f) total error. Radar calibration is assumed corresponding to the global mean SST = 19°C. Calculations are done for V-pol, upwind, and $\theta = 45°$.

component dW_ρ is very similar in the two bands giving similar patterns in Figures 5a and 5d. This wind overestimation is up to 0.3 ms^{-1} over regions where cold SSTs and high winds are both present. But, in many regions wind overestimation due to positive dW_ρ (Figures 5a and 5d) is compensated for by wind underestimation due to negative dW_ν (Figures 5b and 5e). In the C-band, positive dW_ρ and negative dW_ν are of similar magnitudes (Figures 5a and 5b). Hence, combination of the two error components results in a weak total retrieval error overall (Figure 5c). A slight wind overestimation <0.1 ms^{-1} is expected in the C-band over the tropical warm pools and in the 'roaring forties' belt where dW^C = 0.15 ms^{-1} in the Indian Ocean sector (Figure 5c). The total error dW^C is not simply sum of the Taylor series terms $dW_\rho^C + dW_\nu^C$ because of the non-linearity of dW. This is mostly evident over the warm tropical SSTs where $dW^C < dW_\nu^C$, providing dW_ρ^C is negligible (Figures 5a–5c).

[18] At polar latitudes, the total Ku-band error is dominated by ocean viscous effects where SST is cold and winds are moderate (Figure 5f). This leads to wind speed underestimations up to -0.4 ms^{-1} south of 60°S. Viscous effects also dominate in the tropical warm pools with overestimations up to 0.2 ms^{-1} by the Ku-band instrument. As for the C-band scatterometer, the total wind error for the Ku-band scatterometer is smaller than the viscous component $dW < dW^{Ku}$ in the tropics (Figures 5e and 5f) where dW_ν^{Ku} = 0.3 ms^{-1}.

5. Summary

[19] Wind wave energy and radar backscatter vary with SST due to air density-dependence of wind-wave growth rate and temperature dependence in viscous wave dissipation rate. The magnitude of these effects varies with the frequency of the scatterometer. Current empirical scatterometer GMFs do not account for these SST-dependences which can thus preclude climate quality intercalibration of scatterometer winds. To illustrate these impacts on scatterometer wind accuracy, the *Kudryavtsev et al.* [2005] radar imaging model has been used. The results are compared to a set of collocated wind speed estimates from the QuikSCAT and ASCAT instruments. The wind errors are evaluated at vertical polarization in the upwind direction at 45° incidence angle assuming that the radar calibration corresponds to a global mean value of SST = 19°C and that atmospheric stratification is neutral.

[20] The density component of the wind error dW_ρ (due to neglect of temperature-dependence in air density) is very similar for both C- and Ku- frequency bands. According to the model results, wind overestimation due to this error approaches 0.3 ms^{-1} poleward of 40° where cold SSTs and high winds are both present. Wind overestimation can be compensated for by wind underestimation due to neglect of SST-dependence in the viscous wave dissipation rate dW_ν. For the C-band, positive values of dW_ρ and negative values of dW_ν are of similar magnitude. As a result, a weak overestimation <0.1 ms^{-1} is expected over the warm pools of the tropical ocean and in the westerly storm track region of the southern Indian Ocean where the total error dW^C = 0.15 ms^{-1}. The viscous error dominates the total SST-dependent errors for Ku-band scatterometers at polar latitudes where SST is cold but winds are moderate leading to a systematic underestimation, up to -0.4 ms^{-1} south of 60°S, for these instruments using an uncorrected GMF (neglecting SST-dependence). This result is consistent with those presented in *Bentamy et al.* [2012]. In tropical warm pool regions Ku-band instruments will overestimate wind speed by up to 0.2 ms^{-1}.

[21] These wind retrieval errors are based on the model simulation of the direct impact of SST on short wind waves. Although the model provides reasonable agreement with the collocated data, other factors like the impact of the diurnal cycle of winds [e.g., *Lee et al.*, 2008] or partial sea ice could be invoked. At high latitudes the difference between collocated winds is less affected by the diurnal cycle because of the polar convergence of orbits, hence small time delay of collocations. But, the possible impact of partial ice certainly needs further investigation. Moreover, the model does not consider feedback mechanisms related to short scale geometry changes. As coupled, air-water interactions shall affect the wave-induced drag and the friction velocity. These effects are clearly beyond the scope of the present study whose aim is to advocate corrections in the actual scatterometer GMFs to better take into account SST impacts.

[22] **Acknowledgments.** This research was supported by the NASA International Ocean Vector Wind Science Team (NASA NNXIOAD99G). VK and BC acknowledge support provided by Russian Government Mega-grant 11.G34.31.0078. AB acknowledges support provided by the CNES (TOSCA project).

[23] The Editor thanks an anonymous reviewer for assisting in the evaluation of this paper.

References

Beal, R. C., V. N. Kudryavtsev, D. R. Thompson, S. A. Grodsky, D. G. Tilley, V. A. Dulov, and H. C. Graber (1997), The influence of the marine atmospheric boundary layer on ERS 1 synthetic aperture radar imagery of the Gulf Stream, *J. Geophys. Res.*, *102*, 5799–5814, doi:10.1029/96JC03109.

Bentamy, A., S. A. Grodsky, J. A. Carton, D. Croizé-Fillon, and B. Chapron (2012), Matching ASCAT and QuikSCAT winds, *J. Geophys. Res.*, *117*, C02011, doi:10.1029/2011JC007479.

Bourassa, M. A., E. Rodriguez, and R. Gaston (2010), NASA's Ocean Vector Winds Science Team Workshops, *Bull. Am. Meteorol. Soc.*, *91*, 925–928, doi:10.1175/2010BAMS2880.1.

Chelton, D. B., and S.-P. Xie (2010), Coupled ocean-atmosphere interaction at oceanic mesoscales, *Oceanography*, *23*, 52–69, doi:10.5670/oceanog.2010.05.

Donelan, M. A., and W. J. Pierson Jr. (1987), Radar scattering and equilibrium ranges in wind-generated waves with application to scatterometry, *J. Geophys. Res.*, *92*, 4971–5029, doi:10.1029/JC092iC05p04971.

Dunbar, S., et al. (2006), QuikSCAT science data product user manual, version 3.0, *JPL Doc. D-18053–RevA*, Jet Propul. Lab., Pasadena, Calif, [Available at ftp://podaac-ftp.jpl.nasa.gov/allData/quikscat/L2B/docs/QSUG_v3.pdf.]

Ebuchi, N., H. C. Graber, and M. J. Caruso (2002), Evaluation of wind vectors observed by QuikSCAT/SeaWinds using ocean buoy data, *J. Atmos. Oceanic Technol.*, *19*, 2049–2062, doi:10.1175/1520-0426(2002)019<2049:EOWVOB>2.0.CO;2.

Freilich, M. H. (1997), Validation of vector magnitude data sets: Effects of random component errors, *J. Atmos. Oceanic Technol.*, *14*, 695–703, doi:10.1175/1520-0426(1997)014<0695:VOVMDE>2.0.CO;2.

Hersbach, H. (2008), CMOD5.N: A C-band geophysical model function for equivalent neutral wind, *Tech. Memo. 54*, Eur. Cent. for Medium-Range Weather Forecasts, Reading, U K. [Available at http://earth.eo.esa.int/pcs/ers/scatt/articles/CMOD5N.pdf.]

Kudryavtsev, V., and J. Johannessen (2004), On effect of wave breaking on short wind waves, *Geophys. Res. Lett.*, *31*, L20310, doi:10.1029/2004GL020619.

Kudryavtsev, V. N., V. K. Makin, and B. Chapron (1999), Coupled sea surface-atmosphere model: 2, Spectrum of short wind waves, *J. Geophys. Res.*, *104*, 7625–7639, doi:10.1029/1999JC900005.

Kudryavtsev, V., D. Akimov, J. Johannessen, and B. Chapron (2005), On radar imaging of current features: 1. Model and comparison with observations, *J. Geophys. Res.*, *110*, C07016, doi:10.1029/2004JC002505.

Lee, T., O. Wang, W. Tang, and W. T. Liu (2008), Wind stress measurements from the QuikSCAT-SeaWinds scatterometer tandem mission and the impact on an ocean model, *J. Geophys. Res.*, *113*, C12019, doi:10.1029/2008JC004855.

Mouche, A. A., B. Chapron, N. Reul, D. Hauser, and Y. Quilfen (2007), Importance of the sea surface curvature to interpret the normalized radar cross section, *J. Geophys. Res.*, *112*, C10002, doi:10.1029/2006JC004010.

Sharqawy, M. H., V. Lienhard, H. John, and S. M. Zubair (2010), Thermophysical properties of seawater: A review of existing correlations and data, *Desalin. Water Treat.*, *16*, 354–380, doi:10.5004/dwt.2010.1079.

Smith, S. D. (1988), Coefficients for sea surface wind stress, heat flux, and wind profiles as a function of wind speed and temperature, *J. Geophys. Res.*, *93*, 15,467–15,472, doi:10.1029/JC093iC12p15467.

Sobieski, P. W., C. Craeye, and L. F. Bliven (1999), Scatterometric signatures of multivariate drop impacts on fresh and salt water surfaces, *Int. J. Remote Sens.*, *20*, 2149–2166, doi:10.1080/014311699212164.

Stewart, R. W. (1974), The air-sea momentum exchange, *Boundary Layer Meteorol.*, *6*, 151–167, doi:10.1007/BF00232481.

Voronovich, A. G., and V. U. Zavorotny (2001), Theoretical model for scattering of radar signals in Ku- and C-bands from a rough sea surface with breaking waves, *Waves Random Media*, *11*, 247–269, doi:10.1080/13616670109409784.

Weissman, D. E., T. W. Thompson, and R. Legeckis (1980), Modulation of sea surface radar cross section by surface stress: Wind speed and temperature effects across the gulf stream, *J. Geophys. Res.*, *85*, 5032–5042, doi:10.1029/JC085iC09p05032.